Crystal structure of the secreted form of antigen 85C reveals potential targets for mycobacterial drugs and vaccines

Donald R. Ronning[1], Thomas Klabunde[1], Gurdyal S. Besra[2], Varalakshmi D. Vissa[3], John T. Belisle[3] and James C. Sacchettini[1]

The antigen 85 (ag85) complex, composed of three proteins (ag85A, B and C), is a major protein component of the *Mycobacterium tuberculosis* cell wall. Each protein possesses a mycolyltransferase activity required for the biogenesis of trehalose dimycolate (cord factor), a dominant structure necessary for maintaining cell wall integrity. The crystal structure of recombinant ag85C from *M. tuberculosis*, refined to a resolution of 1.5 Å, reveals an α/β-hydrolase polypeptide fold, and a catalytic triad formed by Ser 124, Glu 228 and His 260. ag85C complexed with a covalent inhibitor implicates residues Leu 40 and Met 125 as components of the oxyanion hole. A hydrophobic pocket and tunnel extending 21 Å into the core of the protein indicates the location of a probable trehalose monomycolate binding site. Also, a large region of conserved surface residues among ag85A, B and C is a probable site for the interaction of ag85 proteins with human fibronectin.

The antigenic properties of the antigen 85 (ag85) complex have been studied for more than 30 years[1], yet until recently, the biochemical function was unknown. Antigen 85C was shown to possess a mycolyltransferase enzyme activity, pivotal for the biosynthesis of the mycobacterial cell wall and for the survival of mycobacteria[2]. The importance of the ag85 proteins to cell wall biosynthesis provides a basis for the development of novel antitubercular drugs.

Mycolic acids are long-chain, α-alkyl, β-hydroxyl fatty acids that form a major component of the *Mycobacterium tuberculosis* cell wall[3]. The mycobacterial cell wall is a bilayer in which the outer layer is composed of α, α'-trehalose dimycolate (TDM or cord factor), other noncovalently bound lipids and various proteins, whereas the inner layer is composed of mycolic acids covalently linked to D-arabino-D-galactan and peptidoglycan. Indeed, the cell wall is extremely hydrophobic and confers a level of resistance

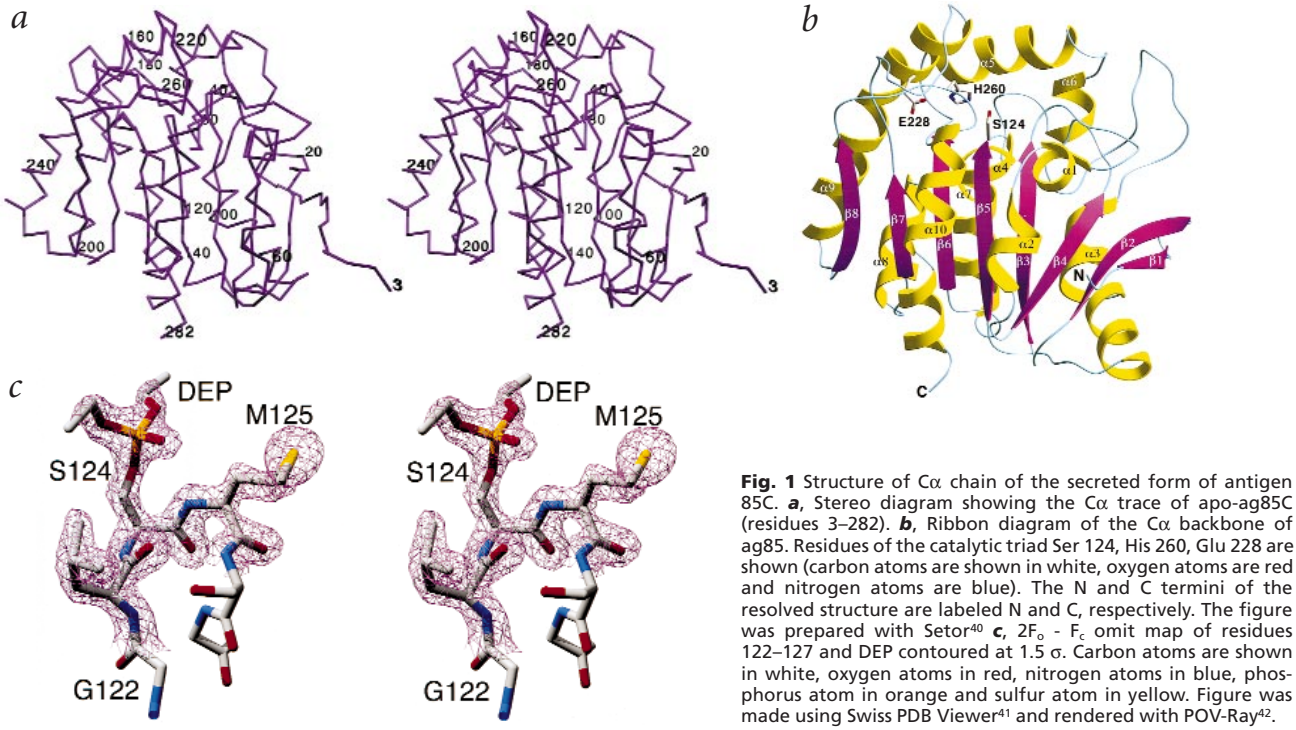

Fig. 1 Structure of Cα chain of the secreted form of antigen 85C. ***a***, Stereo diagram showing the Cα trace of apo-ag85C (residues 3–282). ***b***, Ribbon diagram of the Cα backbone of ag85. Residues of the catalytic triad Ser 124, His 260, Glu 228 are shown (carbon atoms are shown in white, oxygen atoms are red and nitrogen atoms are blue). The N and C termini of the resolved structure are labeled N and C, respectively. The figure was prepared with Setor[40] ***c***, $2F_o$ - F_c omit map of residues 122–127 and DEP contoured at 1.5 σ. Carbon atoms are shown in white, oxygen atoms in red, nitrogen atoms in blue, phosphorus atom in orange and sulfur atom in yellow. Figure was made using Swiss PDB Viewer[41] and rendered with POV-Ray[42].

[1]Department of Biochemistry and Biophysics, Texas A&M University, College Station, Texas 77844-2128, USA. [2]Department of Microbiology and Immunology, University of Newcastle upon Tyne, Newcastle upon Tyne, NE2 4HH, UK. [3]Department of Microbiology, Colorado State University, Fort Collins, Colorado 80523, USA.

Correspondence and requests for material should be addressed to J.C.S. *email: sacchett@tamu.edu*

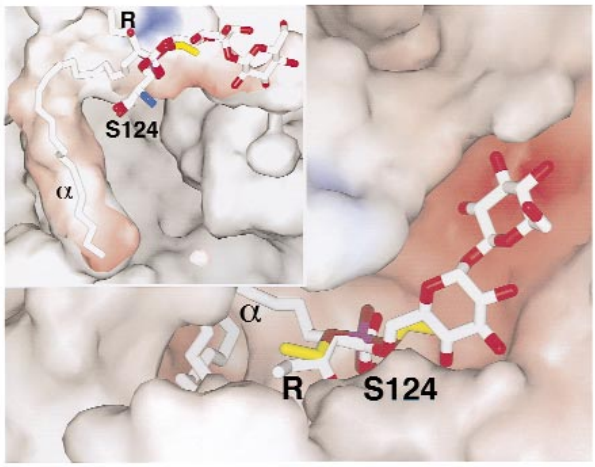

Fig. 2 Proposed binding site for TMM. Superposition of bound DEP and modeled TMM within the substrate binding pocket of ag85C. Carbon atoms of the modeled TMM molecule are white, and the carbon atoms of the DEP molecule are shown in yellow. R represents the β, γ, δ carbons, and the β-hydroxyl of the meromycolate branch; α represents the α-branch of a mycolic acid. The surface is colored by electrostatic potential: The red and blue coloring represent negative and positive electrostatic potential, respectively. Inset, Surface of the binding cleft of a85C highlighting the hydrophobic binding channel that runs through the core of the protein (view created by a 90° rotation along the right/left axis in the paper plane). The image shows how the modeled 24-carbon α-branch of the mycolic acid may fit in this channel. Figure was prepared using SPOCK[43].

of *M. tuberculosis* to the application of traditional antibiotics. In fact, recent evidence shows that the cell wall-linked mycolic acids form the primary barrier for the diffusion of small molecules into the cytoplasm of the cell[4]. Two commonly used antitubercular drugs target enzymes involved in cell wall biosynthesis. Isoniazid, a first-line chemotherapeutic used for the treatment of tuberculosis since 1952[5], kills mycobacteria by inhibiting the biosynthesis of mycolic acids[6,7], whereas ethambutol inhibits the formation of the arabinan component of arabinogalactan and lipoarabinomannan[3,8], both of which form major components of the mycobacterial cell wall.

Ag85C and other members of the ag85 complex catalyze the formation of TDM through the transfer of a mycolic acid from the 6-hydroxyl group of one molecule of trehalose monomycolate (TMM) to the 6'-hydroxyl group of a second molecule of TMM[2]. The effects resulting from the disruption of the ag85c gene or due to inhibition of the ag85c protein have been described[2,4]. A trehalose analog, 6-azido-6-deoxytrehalose, inhibits the mycolyltransferase activity of all three members of the ag85 complex activity *in vitro* and inhibits growth of *Mycobacterium aurum*, indicating the importance of TDM for maintaining the integrity of the *Mycobacterium* cell wall[2]. In addition, removal of TDM from the surface of *M. bovis* bacillus Calmette-Guérin (BCG) by treatment in boiling petroleum ether at 35–60 °C inhibits virulence and persistence in Swiss mice[9]. ag85C has also been shown to be important for the covalent attachment of mycolic acids to the arabinogalactan moiety of the mycobacterial cell wall. A *M. tuberculosis* strain lacking a functional ag85C gene showed a 40% decrease in the amount of cell wall-linked mycolic acid. The ratio between the three types of mycolic acid (α-, methoxy- and ketomycolates) bound covalently to the *M. tuberculosis* cell wall is the same as the parent (H37Rv) strain[4]. This indicates that the loss of ag85C activity, though not specific to only one type of mycolic acid, profoundly affects the amount of product formed. These findings, together with the observation of nearly identical active site residues, lend support to the excellence of the ag85 proteins as targets for new drug development and to the expectation that a single drug might have similar efficacy against all three ag85 proteins. To further aid in the design of new antitubercular drugs targeting the ag85 complex, the crystal structures of ag85C and ag85C with covalently bound inhibitor, diethyl phosphate (DEP), were solved by multiple isomorphous replacement (MIR) methods and molecular replacement, respectively (Table 1).

Structure of antigen 85C

ag85C is a single-domain monomeric protein with dimensions of approximately 46 × 48 × 51 Å. Its main structural feature is an α/β fold (Fig. 1) resembling the *Vibrio harveyi* thioesterase, mammalian pancreatic lipases, acetylcholinesterases, bacterial lipases, and fungal lipases, all of which are members of the α/β-hydrolase superfamily[10]. The central β-sheet contains eight strands (β1, β2, β4, β3, β5, β6, β7, β8) surrounded on both sides by α-helices. The sheet is formed such that the outer two strands, β1 and β8, are oriented perpendicular to each other resulting in a left-handed superhelical twist. The first two strands, β1 and β2, are antiparallel and connected by a hairpin turn. The remainder of the sheet is composed of β-strands running parallel to strand β1 with the strands being connected by either a single, relatively long α-helix, or a series of smaller α-helices.

Location of the active site

The active site is located in a deep cleft running across the carboxyl ends of the central β-sheet (Fig. 2). The helices α5 and α9 form the walls of a large hydrophobic pocket lined by Trp 157, Trp 158, Leu 161, Ile 162, Phe 226 and Leu 227. This pocket leads to the opening of a 21 Å long channel extending through the core of the protein (Fig. 2, inset). The channel formed by Phe 76, Trp 178, Phe 150, Tyr 136 and Ile 132 would allow for extensive hydrophobic interactions between the enzyme and a single acyl group of the substrate, making it well suited to accommodate the shorter α-branch of a mycolic acid. The β-branch of the mycolic acid would fit nicely in a long shallow, partially hydrophobic trough on the surface of the protein.

On the opposite end of the cleft, Trp 262 and a group of residues located on the loop between strand β3 and helix α1 form the putative binding site for the carbohydrate moiety of TMM. This assertion is based not only on its location near the catalytic triad, but also on the size and shape of the pocket. The pocket is an elongated ellipse with a major axis of ~14 Å and a minor axis of 8 Å. In its most extended conformation, trehalose is at most 10.7 × 6.2 Å, indicating that there is ample room for trehalose to bind within this pocket in an orientation similar to that in Fig. 2. Additionally, the side chains of Asp 38, Asn 52, Trp 262 and the backbone atoms of residues Gly 39, Leu 40, Arg 41, Ala 42, Gln 43, Tyr 46, Gly 48 and Ile 51 form a pocket with a highly negative electrostatic potential. The residues that compose the pocket are capable of forming an extensive hydrogen bonding network with the substrate's trehalose moiety as demonstrated by the presence of 10 ordered water molecules within the proposed binding site of both the bound and unbound structures.

As found in other serine esterases, ag85C contains a catalytic triad formed by residues Ser 124, His 260 and Glu 228. These residues are conserved in all of the published ag85 sequences. Ser 124, the nucleophile in the mycolyl transfer reaction, is located at the center of the cleft, separating the putative mycolate and trehalose binding pockets described above (Fig. 2). The serine is posi-

tioned at the tip of a β-strand-turn-helix structural motif termed a 'nucleophile elbow,' which is formed by strand β5 and helix α4 (Fig. 1) and is conserved in all α/β-hydrolases[10]. His 260, located on a loop between strand β8 and helix α10, is perfectly juxtaposed to shuttle protons between the serine nucleophile and the general base Glu 228 (His 261Nε to Ser 125Oγ 2.74 Å and His 260Nδ to Glu 228Oγ 2.76 Å), which is located near the N-terminus of helix α9.

Proposed mechanism

The present work provides a structural basis by which to draw a putative picture of the catalytic mechanism of the mycolyl transfer reaction catalyzed by ag85C (Fig. 3). Consistent with previous mechanistic studies on related serine hydrolases[11,12], Ser 124 is suitably positioned for nucleophilic attack of the carboxyl carbon of the TMM molecule when bound to ag85C. The importance of Ser 124 during catalysis is supported by mutagenesis studies showing that a S124A mutation results in an inactive enzyme[2]. His 260 and Glu 228, the other residues of the catalytic triad, are positioned to assist in the general base-catalyzed attack of the serine nucleophile. The nucleophilic attack by the serine hydroxyl yields an acyl-enzyme intermediate with the mycolic acid covalently attached to Ser 124 (Fig. 3). Related lipases containing covalent adducts with organophosphonate inhibitors have been structurally characterized, supporting the formation of an acyl-enzyme intermediate[13–15].

Following the acylation step, the carbohydrate moiety of the second TMM molecule can bind to the sugar binding site, but would be oriented such that the mycolic acid moiety points in the direction opposite of Ser 124. The proximity of the 6'-hydroxyl of TMM to the catalytic triad would allow for a nucleophilic attack by this group on the carboxylate carbon of the acyl-enzyme intermediate. The resulting tetrahedral transition state collapses upon the protonation of the leaving Ser 124 hydroxyl group. The product, TDM, is formed and the side chain of Ser 124 is released, allowing the enzyme to undergo another cycle of catalysis.

The proposed catalytic mechanism allows for the design of potent antitubercular drugs against the mycolyltransferase activity that irreversibly bind to the active site nucleophile of ag85C. The effectiveness of sulfonyl and phosphoryl inhibitors against serine esterases is well documented[16–18]. These inhibitors are typically analogs of the natural substrate and covalently attach to the active site nucleophile with high efficacy. For example, several new β-lactone derivatives, targeted at lipases possessing an α/β-hydrolase fold, are already available for the treatment of hyperlipidemia and obesity.

Structure of ag85C–DEP complex

In order to gain insights into the enzyme's structure in its bound state, ag85C was reacted with a known α/β-hydrolase inhibitor, diethyl *p*-nitrophenyl phosphate, before crystallization. The unit cell packing of the resulting crystals was significantly altered, and therefore molecular replacement was required to solve the structure. The structure was refined to 1.83 Å resolution (Table 1). The asymmetric unit shows that the single molecule of ag85C has a covalently attached-DEP at the active site serine. The stoichiometry and completeness of binding was confirmed by matrix-assisted laser desorption ionization/mass spectrometry (MALDI-MS) (data not shown).

The superposition of the unliganded form and the DEP-bound ag85C structures resulted in a root mean square (r.m.s) deviation of 0.26 Å (Fig. 4). Indeed the structures are nearly identical except for the region near the proposed acyl binding pocket, which includes the N-terminal half of helix α9, the random coil between strand β7 and helix α9, and a turn containing His 260. The most significant change that occurs upon binding of DEP is the movement of α9 from a highly bent to a nearly straight conformation, resulting in movement of Glu 228 away from the active site. In addition, His 260 rotates away from Ser 124 and occupies the position vacated by Glu 228 to maintain its interaction with that side chain (Fig. 4*a*).

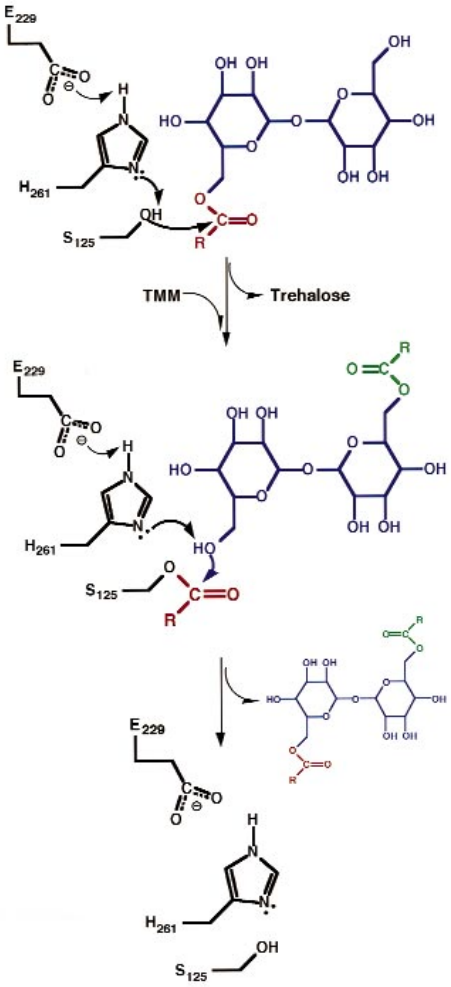

Fig. 3 Schematic representation of the catalytic mechanism of mycolyl transfer. In a three-step reaction, a mycolic acid, shown in red, is transferred from the 6-OH of one molecule of TMM to the 6'-OH of another TMM molecule, forming trehalose and TDM. Protein side chains are shown in black. The carbohydrate moiety of the substrate is in blue. The mycolic acid moiety is represented by a red or green R.

The straightening of helix α9 also moves residues Asp 216 and Leu 217 a distance of 14.1 and 17.8 Å, respectively, from their positions in the unliganded enzyme structure to positions near the active site. This allows the side chain of Leu 217 to occupy the space vacated by His 260, and allows for the formation of hydrogen bonds between the carbonyl oxygens of residues 216 and 217, and for stabilization by bound substrate of the tetrahedral transition state (Fig. 4*a*). The model with TMM bound indicates that the carbonyl oxygen of Leu 217 could hydrogen bond with the β-hydroxyl of the acyl moiety, whereas the Asp 216 carbonyl oxygen could hydrogen bond with O4 of trehalose.

The lack of movement in the remaining portions of ag85C gives additional information pertaining to the catalytic mechanism. The amide protons of residues Leu 40 and Met 125 are 2.66

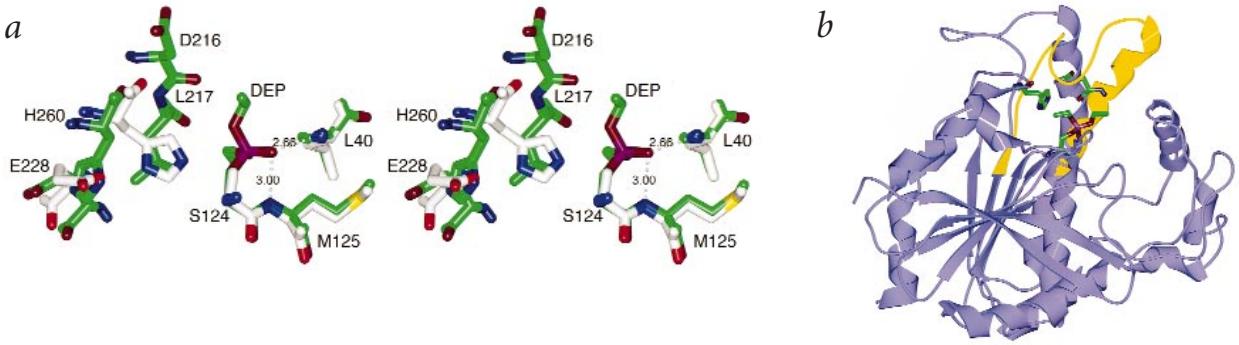

Fig. 4. Superposition of apo-ag85c with DEP-bound ag85C. ***a***, Stereo view of selected active site residues. For the apo form of ag85C, carbon atoms are white, oxygen atoms are red and nitrogen atoms are blue, while the green carbon atoms represent the side chains and DEP from the DEP-bound structure. The dashed gray lines represent the hydrogen bonds formed between the phosphoryl oxygen of DEP and residues forming the oxyanion hole. ***b***, The violet ribbon represents the Cα backbone of apo-ag85C, whereas the yellow ribbon represents the portion of the backbone of the DEP-bound protein that differs from the apo form. The atoms shown represent the catalytic triad, and the DEP of the inhibitor-bound form. Part (*a*) was made using SPOCK[43]; part (*b*) was made using Swiss PDB Viewer[41] and rendered with POV-Ray[42].

and 3.00 Å, respectively, from the phosphoryl oxygen of DEP. These two residues form the oxyanion hole that stabilizes the negative charge of the tetrahedral transition state during catalysis. As Leu 40 and Met 125 remain in the same position in both the apo and bound structures, this implies the presence of a preformed oxyanion hole as seen in the *Fusarium solani pisi* cutinase, indicating that ag85 proteins should resemble cutinase in the sense that interfacial activation is not required for catalytic activity[19,20].

Additionally, residues forming the carbohydrate binding pocket show no conformational differences, indicating that ag85C maintains specificity toward trehalose when in the acyl-enzyme form. The backbone and side chain atoms of residues 38–52, and Trp 262 remain essentially in the same position in both structures, allowing for identical hydrogen bonding interactions between protein and carbohydrate in both the apo and acyl-enzyme forms. This fact adds credence to a single binding site reaction rather than the enzyme requiring multiple sites for catalysis.

Fibronectin binding

In addition to its importance in cell wall biosynthesis, ag85 stimulates the uptake of mycobacteria bacilli by human macrophages. ag85 proteins have been proposed to interact with the gelatin binding site of human fibronectin, resulting in the enhancement of complement-mediated phagocytosis by host macrophages[21–23]. Previous studies on *M. leprae* have shown that the interaction between ag85 and fibronectin is mediated by the sequence homologous to residues 56–66 (FEEYYQSGLSV) of the recombinant *M. tuberculosis* ag85C used in this study[24], a sequence that does not resemble any previously characterized fibronectin binding motif.

In the structure of ag85C, this motif is located on an exposed surface loop connecting helix α2 and strand β4, in agreement with its proposed role in fibronectin binding. Further clues for the location of the molecular area that may be important for fibronectin binding can be derived from a comparison of the ag85 sequences (Fig. 5). A patch of surface residues, identical between the *M. tuberculosis* ag85A, B and C proteins, is found surrounding the proposed fibronectin binding motif (Fig. 5*a*). The patch encompasses 3,271 Å^2, which is 28.4% of the total accessible surface area of the protein. Since the collagen binding domain, which contains the gelatin binding site, of human fibronectin is larger than 45 kDa, it is not unreasonable to imagine all, or nearly all, of this conserved patch as being responsible for fibronectin binding. Further studies are needed to

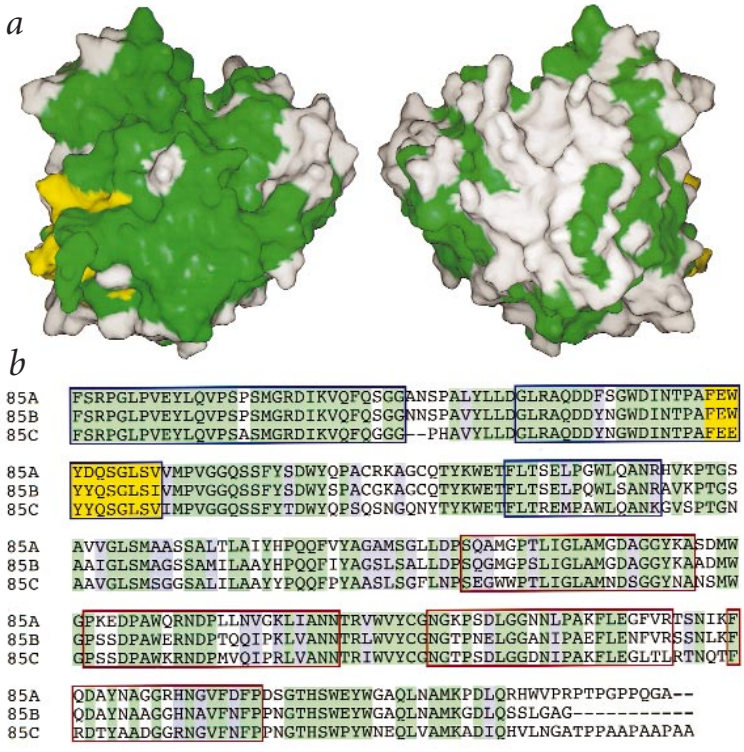

Fig. 5. Fibronectin binding region and multiple sequence alignment of the three *M. tuberculosis* antigen 85 proteins. ***a***, The surfaces shown are rotated 180°, along the vertical axis running through the page, to each other. The green regions represents identical residues within the ag85A, B and C proteins, while the white surfaces show nonidentical residues. The yellow region represents the region found by Naito *et al.*[24] to be involved in fibronectin binding. ***b***, Multiple sequence alignment. Residues conserved in all three proteins are highlighted in green. Similar residues are highlighted in violet. Residues previously shown to be involved in fibronectin binding are highlighted in yellow. Sequences enclosed by blue boxes represent regions involved in fibronectin binding. Sequences enclosed by a red rectangle represent regions containing large continuous stretches of solvent-exposed residues and high sequence identity between the three *M. tuberculosis* antigen 85 proteins. The surfaces were made using SPOCK[43]. The sequence alignment was made using ClustalW[44].

Table 1 Phasing and refinement statistics

Diffraction data

Data Set	Resolution (Å)	Completeness (%) (total / highest)	No. of reflections (total / unique)	I/σI	R_{sym}[1] (overall / highest)	Phasing power[2] (acentric / centric)
pHMPS + DTT	30–2.26	98.0 / 94.4	120,486 / 15,002	9.1	0.083 / 0.165	–
pHMPS1	30–2.26	98.4 / 94.3	163,166 / 15,218	13.5	0.061 / 0.233	1.489 / 1.979
pHMPS2	30–2.10	98.2 / 98.2	158,007 / 19,521	11.5	0.061 / 0.271	1.901 / 2.777
pHMPS/$K_3UO_2F_5$	30–2.60	53.5 / 55.3	21,844 / 9,858	12.7	0.065 / 0.169	1.324 / 1.516
pHMPS/$K_3UO_2F_5$	30–2.30	98.7 / 98.9	116,364 / 14,405	10.6	0.074 / 0.328	2.169 / 2.871
$K_3UO_2F_5$	30–2.40	97.7 / 97.3	97,552 / 12,684	9.9	0.078 / 0.311	1.734 / 2.310
Native 1[3]	30–2.50	95.4 / 90.4	208,129 / 29,775	10.7	0.070 / 0.153	–
Native 2[4]	20–1.5	96.9 / 99.2	425,433 / 110,059	11.5	0.045 / 0.276	–
DEP	30–1.83	94.4 / 80.3	128,115 / 27,884	15.5	0.052 / 0.226	–

Refinement statistics

	Apo form	DEP-bound form
Resolution (Å)	20–1.5	30–1.83
Reflections in working set	104,747	24,284
R_{cryst} (%)	16.63	16.83
R_{free} (%)	18.49	18.82
R.m.s.d. bond lengths (Å)	0.015	0.005
R.m.s.d. bond angles (°)	1.70	1.24
Average B factor (Å²)	19.83	21.02

[1]$R_{sym} = \Sigma | I - \langle I \rangle | / \Sigma \langle I \rangle$, where I is the observed intensity, and $\langle I \rangle$ is the average intensity of multiple observations of symmetry-related reflections.
[2]Phasing power = $\Sigma |F_{H(calc)}| / \Sigma |E|$, where F_H is the structure factor of the heavy atoms and E (lack of closure error) = $|F_{PH(obs)}| - |F_{PH(calc)}|$. Phase calculations were performed using data between 30 and 2.7 Å.
[3]Data set used for molecular replacement and initial model refinement.
[4]Data set used for final model refinement.

determine the exact nature of the interactions between ag85 and the gelatin binding site of human fibronectin.

Antigenic properties

As the predominant secreted proteins of pathogenic mycobacteria, with ag85 composing anywhere from 14 to 60% of the total protein found in culture fluid[25–27], researchers have continued to focus on the antigenic properties of the ag85 protein[28,29] Although ag85 proteins are secreted and subsequently released to culture, they are also found associated with the surface of mycobacteria[29]. This transient localization to the mycobacterial cell wall may explain why live vaccines elicit an immune response to ag85 proteins while killed vaccines do not[30]. However, research has shown that one can induce, using ag85 proteins, alone or in combination with other secreted *M. tuberculosis* proteins, strong cell-mediated immune responses and protective immunity in a guinea pig model system[29]. As guinea pigs are highly susceptible to pulmonary tuberculosis, this research indicates that peptide mimetics of the three ag85 proteins may induce immunoprotection in humans. In addition, Roche *et al.* demonstrated that a specific T-cell reactive peptide designed using the *M. bovis* ag85B sequence as a model is recognized by 87% of BCG vaccines and 93% of tuberculosis patients, while another peptide was recognized by 73% of people in both groups[28]. However, other reports indicate that ag85A and B contain different epitopes from ag85C (ref. 31), which implies that different peptide sequences may be necessary to produce antibodies against all three ag85 proteins. The structure of ag85C sheds light on the regions of the ag85 proteins that may act as epitopes, and allows for the rational design of peptide mimetics that stimulate antibody production against these and other surface sequences.

The most effective mimetics would resemble surface sequences involved in fibronectin binding. In fact, the two sequences recognized by BCG vaccines and TB patients correspond to two of the three sequences implicated in this study to interact with fibronectin. Antibodies against these regions would effectively occlude one of the gateways *M. tuberculosis* uses to enter host macrophages. In addition, other surface sequences not involved in fibronectin binding but containing high sequence similarity between the three ag85 homologs (Fig. 5*b*) would represent good candidates for vaccine design. Peptides of two conserved sequences, 188–212 and 238–255, and the proposed fibronectin binding sequences are currently being synthesized to test the usefulness of these sequences in eliciting an immune response and for vaccine design.

Methods

Data collection. Recombinant ag85C was purified[2], then crystallized in 100 mM sodium citrate pH 5.6, 0.7 M $NH_4H_2PO_4$ using the hanging-drop vapor diffusion method. Crystals were obtained in the orthorhombic space group $P2_12_12_1$ with unit cell dimensions a = 67.7 Å, b = 75.9 Å and c = 137.4 Å (pHMPS- form) and two molecules in the asymmetric unit (solvent content ~53%). In the presence of 1 mM pHMPS, nonisomorphous crystals formed in $P2_12_12_1$ with unit cell dimensions a = 61.8 Å, b = 68.3 Å and c = 75.3 Å (pHMPS+ form) and one monomer per asymmetric unit. The pHMPS+ form crystals proved to be more stable against soaking with heavy atom compounds. Incubation of a pHMPS+ form crystal in 2 mM dithiothreitol (DTT), 100 mM sodium citrate pH 5.6, 0.7 M $NH_4H_2PO_4$ removed the mercury, providing a native crystal for the pHMPS+ form. Further derivatives were obtained by soaking the pHMPS+ crystals with 5 mM $K_3UO_2F_5$ with and without the presence of 2 mM DTT. DEP-bound protein was produced by reacting 600 μl of 10 mg ml^{-1} of an ag85C solution buffered by a 10 mM Tris solution at pH 7.5 with 1 μl of diethyl *p*-nitrophenyl phosphate (DPNP, Sigma), resulting in roughly a two-fold molar excess of DPNP. The reaction was incubated for 12 h at 4 °C, then subjected to a desalting column to remove unreacted DPNP. This protein was concentrated to 10 mg/ml and used for crystallization studies. Crystals of the DEP-bound form grew in 100 mM sodium citrate, 30% 2-methyl-2,4-pentanediol and 200 mM ammonium acetate. Initial diffraction data were collected at room temperature on a NONIUS/MACSCIENCE DIP2030 image plate detector, using a RIGAKU rotating-anode X-ray source. Data

were reduced with DENZO and SCALEPACK[32]. For all data sets intensities were converted to structure factors using TRUNCATE[33] or PHASES[34]. The data set extending to 1.5 Å was collected at the SBC beamline at the Advanced Photo Source in the Argonne National Laboratory. Data were collected on a Mosaic CCD detector using 1 Å wavelength X-rays. Data were reduced using HKL2000[32], and converted to structure factors using CNS[35].

Structure determination and refinement. The mercury position was initially obtained from isomorphous Patterson maps calculated in PHASES[34]. The binding site of the second derivative, $K_3UO_2F_5$, was obtained from difference Fourier maps using phase information calculated from the pHMPS derivative. The heavy atom positions were refined in MLPHARE[33], and MIR phases were computed using SHARP[36]. Phase refinement proceeded with DM[33,37] using solvent flattening and histogram matching. Successive rounds of model building in the program O[38] with refinement of the partial structure using CNS[35] and phase combination using SIGMAA[33] allowed for an unambiguous tracing of the protein from residues 3 to 282. The pHMPS+ structure provided a search model to obtain phase information for the pHMPS- form of ag85C by molecular replacement methods using AMoRe[39]. The slow cooling protocol in CNS[35] was used to refine the structure to a resolution of 1.5 Å. The final structure was refined using successive rounds of model manipulation and positional refinement, and is missing 3 N-terminal and 12 C-terminal residues. Water molecules were added using CNS[35] and by inspection of F_o - F_c maps. The final refined structure has good stereochemistry, with the Ramachandran plot showing 88.9% of the residues in the core allowed regions and two residues in the disallowed or generously allowed regions, and contains 4,943 atoms including 583 water molecules. The active site serine, Ser 124, which is commonly found in disallowed regions, represents one of the two residues possessing poor stereochemistry. The second residue, Ser 86, is found at a sharp turn on a loop of random coil, so the poor stereochemistry may be a result of the tight turn. The molecular replacement protocol from CNS[35] was used to obtain phases for the DEP-bound crystal form. A monomer of the apo form of ag85C was used as a search model. Rigid body refinement was performed using the translation solution. A refinement procedure similar to that used for the apo model was also used to refine the DEP model. The final model of 2,521 atoms, including 299 water molecules, one DEP molecule, and two molecules of MPD, has good stereochemistry, with the Ramachandran plot showing 87.9% of the residues in the core allowed regions and two residues in the disallowed or generously allowed regions.

Coordinates. Coordinates have been deposited in the protein Data Bank (accession codes 1DQY and 1DQZ).

Acknowledgments

Financial support was provided by the Robert A. Welch Foundation and the NIH. We would like to thank the staff of the SBC-CAT at the APS at Argonne National laboratory, specifically, Frank Rotella for all of his help with data collection.

Received 24 September, 1999; accepted 16 December, 1999.

1. Fukui, Y., Hirai, T., Uchida, T. & Yoneda, M. Extracellular proteins of tubercle bacilli. IV. Alpha and beta antigens as major extracellular protein products and as cellular components of a strain (H37Rv) of *Mycobacterium tuberculosis*. *Biken J.* **8**, 189–199 (1965).
2. Belisle, J.T. *et al*. Role of the major antigen of *Mycobacterium tuberculosis* in cell wall biogenesis. *Science* **276**, 1420–1422 (1997).
3. Brennan, P.J. & Nikaido, H. The envelope of mycobacteria. *Annu. Rev. Biochem.* **96**, 29–63 (1995).
4. Jackson, M. *et al*. Inactivation of the antigen 85C gene profoundly affects the mycolate content and alters the permeability of the *Mycobacterium tuberculosis* cell envelope. *Mol. Microbiol.* **31**, 1573–1587 (1999).
5. Robitzek, E.H. & Selikoff, I.J. Hydrazine derivatives of isonicotinic acid (Rimifon, Marsilid) in the treatment of active progressive caseous–pneumonic tuberculosis. *Am. Rev. Tuberc. Pulm. Dis.* **65**, 765 (1952).
6. Blanchard, J.S. Molecular mechanisms of drug resistance in *Mycobacterium tuberculosis*. *Annu. Rev. Biochem.* **65**, 215–239 (1996).
7. Banerjee, A. *et al*. *inhA*, a gene encoding a target for isoniazid and ethionamide in *Mycobacterium tuberculosis*. *Science* **263**, 227–230 (1994).
8. Takayama, K.& Kilburn, J.O. Inhibition of synthesis of arabinogalactan in *Mycobacterium smegmatis*. *Antimicrob Agents Chemother.* **33**, 1493–1499 (1989).
9. Silva, C.L., Ekizlerian, S.M. & Fazioli, R. Role of cord factor in the modulation of infection caused by mycobacteria. *Am. J. Pathol.* **118**, 238–247 (1985).
10. Schrag, J.D. & Cygler, M. Lipases and α/β hydrolase fold. *Methods Enzymol.* **284**, 85–107 (1997).
11. Powers, J.C. *et al*. Proteases—structures, mechanism and inhibitors. *Agents Actions Suppl*. **42**, 3–18 (1993).
12. Kraut, J. Serine proteases: structure and mechanism of catalysis. *Annu. Rev. Biochem.* **46**, 331–358 (1977).
13. Egloff, M.P. *et al*. The 2.46 Å resolution structure of the pancreatic lipase–colipase complex inhibited by a C11 alkyl phosphonate. *Biochemistry* **34**, 2751–2762 (1995).
14. Uppenberg, J. *et al*. Crystallographic and molecular-modeling studies of lipase B from *Candida antarctica* reveal a stereospecificity pocket for secondary alcohols. *Biochemistry* **31**, 16838–16851 (1995).
15. Bullock, T.L., Breddam, K. & Remington, S.J. Peptide aldehyde complexes with wheat serine carboxypeptidase II: implications for the catalytic mechanism and substrate specificity. *J. Mol. Biol*. **255**, 714–725 (1996).
16. Ransac, S. *et al*. Covalent inactivation of lipases. *Methods Enzymol.* **286**, 190–231 (1997).
17. Leuveling Tjeenk, M. *et al*. Inactivation of *Staphylococcus hyicus* lipase by hexadecylsulfonyl fluoride: evidence for an active site serine. *Protein Eng.* **7**, 579 (1994).
18. Maylie, M.F., Charles, M. & Desnuelle P. Action of organophosphates and sulfonyl halides on porcine pancreatic lipase. *Biochim. Biophys. Acta* **276**, 162–175 (1972).
19. Longhi, S., Czjzek, M., Lamzin, V., Nicolas, A. & Cambillau C. Atomic resolution (1.0 Å) crystal structure of *Fusarium solani* cutinase: stereochemical analysis. *J. Mol. Biol*. **268**, 779–799 (1997).
20. Martinez, C. Cutinase, a lipolytic enzyme with a preformed oxyanion hole. *Biochemistry* **33**, 83–89 (1994).
21. Abou-Zeid, C. *et al*. Characterization of fibronectin-binding antigens released by *Mycobacterium tuberculosis* and *Mycobacterium bovis* BCG. *Infect. Immun*. **56**, 3046–3051 (1988).
22. Schlesinger L.S. & Horowitz, M.A. Phagocytosis of *Mycobacterium leprae* by human monocyte-derived macrophages is mediated by complement receptors CR1 (CD35), CR3 (CD11b/CD18), and CR4 (CD11c/CD18) and IFN-γ activation inhibits complement receptor function and phagocytosis of this bacterium. *J. Immunol*. **147**, 1983–1994 (1991).
23. Schorey, J.S., Carroll, M.C. & Brown, E.J. A macrophage invasion mechanism of pathogenic mycobacteria. *Science* **277**, 1091–1093 (1997).
24. Naito, M., Ohara, N., Matsumoto, S. & Yamada, T. The novel fibronectin-binding motif and key residues of mycobacteria. *J. Biol. Chem.* **273**, 2905 (1998).
25. De Bruyn, J., Bosmans, R., Nyabenda, J. & Van Vooren, J.P. Effect of zinc deficiency on the appearance of two immunodominant protein antigens (32 kDa and 65 kDa) in culture filtrates of mycobacteria. *J. Gen.* **135**, 79–84 (1989).
26. Fukui, Y., Hirai, T., Uchida, T. & Yoneda, M. Extracellular proteins of tubercle bacilli. IV. Alpha and beta antigens as major extracellular protein products and as cellular components of a strain (H37Rv) of *Mycobacterium tuberculosis*. *Biken J.* **8**, 189–199 (1965).
27. Wiker, G.H. & Harboe, M. The antigen 85 complex: a major secretion product of *Mycobacterium tuberculosis*. *Microbiol. Rev.* **56**, 648–661 (1992).
28. Roche, P.W., Peake, P.W., Billman-Jacobe, H., Doran, T. & Britton, W.J. T-Cell determinants and antibody binding sites on the major mycobacterial secretory protein MPB59 of *Mycobacterium bovis*. *Infect. Immun.* **62**, 5319–5326 (1994).
29. Horwitz, M.A., Lee, B.W., Dillon, B.J. & Harth, G. Protective immunity against tuberculosis induced by vaccination with major extracellular proteins of *Mycobacterium tuberculosis*. *Proc. Natl. Acad. Sci. USA* **92**, 1530–1534 (1995).
30. Orme, I.M. Characteristics and specificity of acquired immunologic memory to *Mycobacterium tuberculosis* infection. *J. Immunol.* **140**, 3589–3593 (1988).
31. Samanich, K.M. *et al*. Delineation of human antibody responses to culture filtrate antigens of *Mycobacterium tuberculosis*. *J. Infect. Dis.* **178**, 1534–1538 (1998).
32. Otwinowski, Z. & Minor, W. Processing of X-ray diffraction data collected in oscillation mode. *Methods Enzymol*. **27**, 307–326 (1997).
33. Collaborative Computational Project, Number 4. CCP4 Suite: programs for protein crystallography. *Acta Crystallogr. D* **50**, 760–763 (1994).
34. Furey, W. & Swaminathan, S. PHASES. *Am. Crystallogr. Assoc. Annu. Mtg. Program. Abstr.* **18**, 73 (1990).
35. Brünger, A.T. *et al*. Crystallography & NMR system (version 0.9): a new software suite for macromolecular structure determination. *Acta Crystallogr. D* **54**, 905–921 (1998).
36. de La Fortelle, E. & Bricogne, G. Maximum-likelihood heavy atom parameter refinement for the multiple isomorphous replacement and multiwavelength anomalous diffraction methods. *Methods Enzymol.* **276**, 472–494 (1997).
37. Cowtan, K.D. & P. Main, P. Phase combination and cross validation in iterated density-modification calculations. *Acta Crystallogr. D* **52**, 43–48 (1996).
38. Jones, T.A., Zou, J.Y., Cowan, S.W. & Kjeldgaard, M. Improved methods for building protein models in electron density maps and the location of errors in these models. *Acta Crystallogr. A* **47**, 110–119 (1991).
39. Navaza, J. AMoRe: an Automated Package for Molecular Replacement. *Acta Crystallogr. A* **50**, 157–163 (1994).
40. Evans, S.V. Setor: hardware lighted three-dimensional solid model representations of macromolecules. *J. Mol. Graph.* **11**, 134–138 (1993).
41. Guex, N. & Peitsch, M.C. SWISS-MODEL and the Swiss-PdbViewer: an environment for comparative protein modeling. *Electrophoresis* **18**, 2714–2723 (1997).
42. Amundsen, S. *et al*. X-POV-Team POV-Ray: persistence of vision ray-tracer. http://www.povray.org (1997).
43. Christopher, J.A. *SPOCK: the structural properties observation and calculation kit* (program manual). (The Center for Macromolecular Design, Texas A&M University, College Station, Texas; 1998).
44. Higgins, D.G., Bleasby, A.J. & Fuchs, R. CLUSTAL V: improved software for multiple sequence alignment. *Comput. Applic. Biosci.* **8**, 189–191 (1992).